Resilience of riverbed vegetation to uprooting by flow

PROCEEDINGS
OF THE ROYAL SOCIETY A
MATHEMATICAL, PHYSICAL AND ENGINEERING SCIENCES

Resilience of riverbed vegetation to uprooting by flow

P. Perona[1] and B. Crouzy[2]

[1]Institute for Infrastructure and Environment, School of Engineering, The University of Edinburgh, UK
[2]Federal Office of Meteorology and Climatology, MeteoSwiss, Payerne, CH

Riverine ecosystem biodiversity is largely maintained by ecogeomorphic processes including vegetation renewal via uprooting and recovery times to flow disturbances. Plant roots thus heavily contribute to engineer resilience to perturbation of such ecosystems. We show that vegetation uprooting by flow occurs as a fatigue-like mechanism, which statistically requires a given exposure time to imposed riverbed flow erosion rates before the plant collapses. We formulate a physically-based stochastic model for the actual plant rooting depth and the time-to-uprooting, which allow us to define plant resilience to uprooting for generic time-dependent flow erosion dynamics. This theory shows that plant resilience to uprooting depends on the time-to-uprooting and that root mechanical anchoring acts as a process memory stored within the plant-soil system. The model is validated against measured data of time-to-uprooting of *Avena sativa* seedlings with various root lengths under different flow conditions. This allows for assessing the natural variance of the uprooting-by-flow process and to compute the prediction entropy, which quantifies the relative importance of the deterministic and the random components affecting the process.

Proc. R. Soc. A.royalsocietypublishing.org

Research

Article submitted to journal

Subject Areas:
Environmental engineering, Hydrology, Civil Engineering

Keywords:
Plant uprooting, flow erosion, stochastic process, type II uprooting, resilience to uprooting

Author for correspondence:
P. Perona
e-mail: paolo.perona@ed.ac.uk

1. Introduction

Riverine corridors are known to host the highest degree of biodiversity among all ecosystems [1]. At the ecotone scale, this is the result of interactions of riparian vegetation, sediment and flow processes. Hydrological variability controls such ecogeomorphic processes [2,3] via thresholds and both positive and negative feedbacks occurring over multiple timescales (e.g., see [4] for a review). In this fully coupled eco-geomorphological system the feedback from vegetation biomass is particularly strong. As vegetation contributes to engineer specific niches of biological importance for both aquatic and terrestrial lifeforms [5], flood-induced mortality is a key component of ecomorphodynamic process complexity. Such complexity is believed to have developed following the slow evolution of plant roots starting in the Palaeozoic, which changed drastically the sediment erosion and deposition dynamics [6] and, in turn, resistance of vegetation to uprooting by flow. In this work we frame the ability of plant roots to withstand uprooting under the concept of resilience, which is yet rather poorly defined for environmental processes. We will show that resilience to uprooting is a concept naturally connected with the probability of uprooting and its predictability.

To some extent, riparian plants may adjust their root structure to adapt to water and oxygen availability [7,8] through tropic responses (e.g., see [9] for details). Hence, oxitropic response to generically high groundwater levels determines shallow roots, whereas hydrotropic response to catch low groundwater levels forces roots to grow deeper in the alluvial sediment [7]. The root network also contributes to sediment stabilization [10,11]. During flood events, flow induced plant uprooting results from both flow drag and scouring that gradually reduces the mechanical anchoring of roots [12–14]. This process appears remarkably similar over a range of scales but its physics is still far from being completely understood (Figure 1).

Many environmental dynamics are characterized by a strong deterministic component coupled to process noise and have been modelled by means of stochastic approaches (e.g., see [15,16]). Static uprooting of plants revealed an almost monotonically growing stress-strain curve characterized by a clear elastic response [17,18]. The effect of process noise emerges in the descending phase of the curve as a result of load redistribution among sliding and sequentially tensioned roots, as well as from readjustment of the soil-root matric grains [14,19–21]. In river corridors, plants exposed to flood events are not really pulled out of the soil by hydrodynamic drag forces only, except for seedlings or re-sprouted woody debris at very early stages of growth (named Type I uprooting, after Edmaier *et al.* [12]). The establishment of seedlings is controlled by a selection mechanism where uprooting often occurs within a single flood event [22,23]. Plant stem size and density shift the length scales of turbulence eddies towards small scales, thus increasing the fluctuation in the hydrodynamic forces due to fluid-plant interactions [24]. This makes the uprooting process Type I suitable for study by stochastic methods [22,25]. At later stages of growth, however, the increased root mechanical anchoring delays the uprooting process to multiple flow events, and the ability of plants to recover between them becomes essential [26]. Uprooting thus occurs in conjunction with either local or non-local sediment erosion at the stem base (named Type II after Edmaier *et al.* [12]). As scouring proceeds during high flows, plant roots are gradually exposed, mechanical anchoring decreases until it balances flow drag and then uprooting occurs [12]. Edmaier *et al.* [27] investigated experimentally Type II erosion at the laboratory scale using *Avena sativa* as prototype of riverbed vegetation. Although this species is not a riparian species, it has been widely used in previous laboratory flume experiment. Hence, at that scale, Edmaier *et al.* showed that contrarily to pullout experiments, Type II uprooting dynamics is influenced by the exposure time to riverbed erosion rate and to a large random component.

In the following, we build on the concepts outlined by Edmaier *et al.* [27] and address from a quantitative point of view the conditioning of vegetation uprooting to sequential flow erosion events. We mathematically model the Type II uprooting mechanism as a (deterministic) mechanical fatigue perturbed by a (random) process noise, where plant collapsing occurs after a

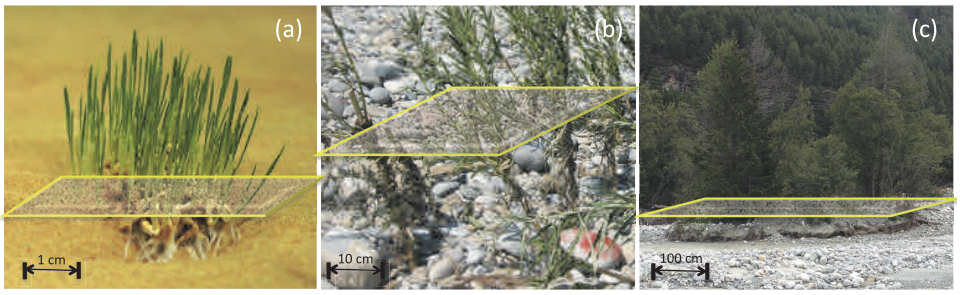

Figure 1. Examples of local and non-local riverbed erosion exposing vegetation roots at different scales. The horizontal plane shows the approximate location of riverbed elevation before deep erosion occurred. a) Local scouring around a patch of *Avena sativa* seedlings after a flooding event in a flume experiment; b) non-local scour within a plot of willow cuttings after a flood on a gravel island of Thur River, Canton Thurgau, Switzerland (from [29]); c) patch of mature trees showing large scale non-local riverbed erosion as well as sediment stabilization by roots, Borgne River, Val d'Hérens, Switzerland.

given exposure time to riverbed scouring reducing the rooting depth. As uprooting depends on the root architecture within the soil, we first compute the energy spent by the stream to reduce the rooting depth in time and use it as a proxy for defining the resilience to uprooting. The ability to predict uprooting following flow events is then framed by using the prediction entropy [16], which is defined as the base two logarithm of the probability of plant uprooting being the latter interpreted as a binary (i.e., on-off) process. This stochastic modelling framework is validated by using the experimental dataset of [28] on *Avena sativa* seedlings. By this means, the model allows us to identify explicitly the relative importance of the deterministic and random components in such a memory-like process affecting the plant-soil system.

2. Mathematical model

We proceed by first building the mathematical structure of stochastic flow erosion that reduces plant mechanical anchoring and then present some exemplary analytical solutions for the probability density functions of the actual rooting depth and the time to uprooting. This will allow us to define the resilience to uprooting under a probabilistic frame.

(a) Process equation

Root mechanical anchoring depends largely on the rooting depth, L [17,18]. Accordingly, we formulate a simple stochastic model for the evolution of $L(t)$ with bed elevation changes as erosion and deposition take place and assuming the plant does not grow during a flooding event. At the plant scale (e.g., see Figure 2), we assume the variable $L(t)$ being a function, f, of the mean soil elevation burying the roots, $\bar{\eta}(x^*, t)$

$$L(t) = f(\bar{\eta}(t; x^*)), \tag{2.1}$$

where t is time and x^* is the spatial location of the plant. In this model, x^* plays the role of a parameter as the vertical root density is location dependent. Together with the rooting depth the vertical root density statistics determine how the rooting length (and therefore mechanical anchorage) changes with soil depth. We assume here that root mechanical anchoring equals flow drag when the rooting depth reaches a critical value, L_c. The function, f describes how the actual rooting depth changes with soil elevation because of morphogenic processes (i.e., erosion and deposition). By computing the time derivative of eq.(2.1), we obtain

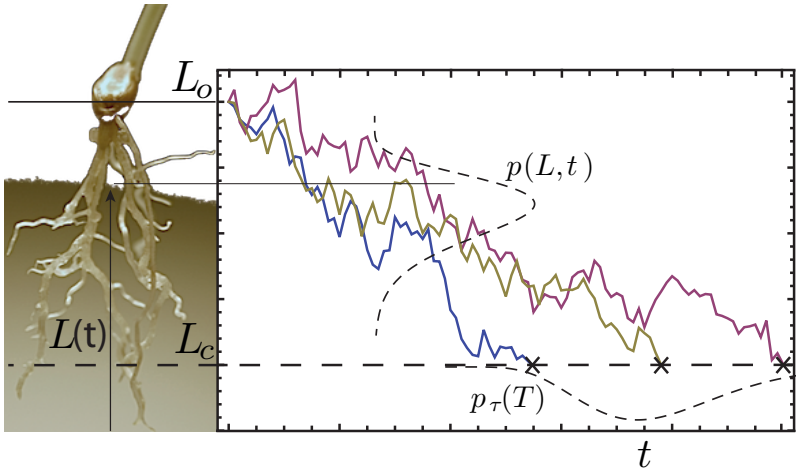

Figure 2. Illustration of the process described by Eq. (2.9). The state variable L evolves following a deterministic drift and a random white noise ($\frac{v_{sed}}{\sigma} = 4$, lengthscale and timescale arbitrary). Once the critical state L_c is reached, the trajectory is lost (uprooting for the situation considered in this paper). The probability density functions $p(L,t)$ and $p_\tau(T)$ describe the statistics of the ensemble of trajectories and of the first passage time across the boundary at L_c, respectively.

$$\frac{dL}{dt} = \frac{df}{d\bar{\eta}}\frac{d\bar{\eta}}{dt}. \tag{2.2}$$

The evolution of soil elevation is obtained first by considering the Exner equation for local (i.e., around x^*) bed elevation changes

$$(1-\lambda)\frac{\partial \eta}{\partial t} = -\frac{\partial Q_s}{\partial x}, \tag{2.3}$$

which links sediment volume spatial rate, $Q_s(x,t)$ to local bed elevation changes in time. We now integrate the Exner equation spatially between two sections, 1 and 2 located at $x^* \pm S/2$, i.e. around the plant, with S assumed of the order of the plant size

$$(1-\lambda)\int_1^2 \frac{\partial \eta}{\partial t}dx = -\int_1^2 \frac{\partial Q_s(x,t)}{\partial x}dx. \tag{2.4}$$

By bringing the time derivative outside the integral and by introducing the mean soil elevation over a distance S, $\bar{\eta}(t) = \frac{1}{S}\int_1^2 \eta(x,t)dx$ we obtain

$$(1-\lambda)S\frac{d\bar{\eta}}{dt} = -[Q_{s,2}(t) - Q_{s,1}(t)]. \tag{2.5}$$

Net bed erosion during flooding events occurs if $Q_{s,1} \ll Q_{s,2}$, by which means, at the first order eq.(2.5) becomes

$$\frac{d\bar{\eta}}{dt} = -\frac{1}{S(1-\lambda)}Q_{s,2}(t)\left(1 - \frac{Q_{s,1}(t)}{Q_{s,2}(t)}\right) \simeq -\frac{1}{S(1-\lambda)}Q_{s,2}(t). \tag{2.6}$$

The sediment rate, $Q_{s,2}$ is per se a fluctuating quantity as it depends on bed shear stress and, ultimately on flow velocity, U according to some closure bedload formulas. Flow velocity fluctuates according to the turbulent flow and the presence of the plant as shown by Nepf [24]. Such fluctuations affect the local transport of sediment thus contributing to its well known irregular nature. Hence, we perform the Reynolds decomposition for $Q_{s,2}$ in order to separate the mean transport from fluctuations around it over a turbulent characteristic time, which is typically

much shorter than the hydrologic event duration,

$$\frac{d\bar{\eta}}{dt} = -\frac{1}{S(1-\lambda)}[\bar{Q}_{s,2}(t) + Q'_{s,2}(t)]. \tag{2.7}$$

The first term on the right hand side is responsible for the mean erosion/deposition trend, whereas the second one accounts for fluctuations induced by flow turbulence, fluid obstacle interactions and the sediment movement dynamic due to grain-grain interactions. By plugging eq (2.7) into eq (2.2) we have

$$\frac{dL}{dt} = -\frac{df}{d\bar{\eta}}\frac{1}{S(1-\lambda)}\bar{Q}_{s,2}(t) + \frac{df}{d\bar{\eta}}\frac{1}{S(1-\lambda)}\Xi(t), \tag{2.8}$$

where we set $\Xi(t) = -Q'_{s,2}(t)$ in order to take into account that a positive fluctuation of Q'_2 around the mean, $\bar{Q}_{s,2}$ reduces the erosion rate. The derivative $df/d\eta$ introduces a dependence on the rooting length, L on both terms of eq. (2.8). As far as the first term on the right-hand side is concerned we set $v_{sed}(L,t) = \frac{df}{d\bar{\eta}}\frac{1}{S(1-\lambda)}\bar{Q}_{s,2}(t)$. The fluctuating term, $\Xi(t)$ is a noise term with *a priori* unknown properties modulated by a term $\nu(L,t) = \frac{df}{d\bar{\eta}}\frac{1}{S(1-\lambda)}$. Eventually, the rooting length $L(t)$ evolves from the initial main rooted depth length $L(0) = L_0$, according to a Langevin equation of the form [30],

$$\frac{dL}{dt} = -v_{sed}(L,t) + \nu(L,t)\Xi(t), \qquad t > 0, \tag{2.9}$$

that is the rooting depth evolves as a result of deterministic drift, v_{sed} describing the mean erosion dynamics, and multiplicative process noise, Ξ accounting for local fluctuations of the erosion/deposition processes. Generally, this equation should be coupled to a morphodynamic model that returns the functions $v_{sed}(L,t)$, whereas the nature of the noise and of the multiplicative term $\nu(L,t)$ should be determined experimentally. However, if the scouring process occurs at a spatial scale much larger than the obstacle size, then parallel riverbed erosion can be assumed as an approximation [27]. Notice, that this condition is equivalent to assume a sediment-to-obstacle size ratio close to unity [31], which implies negligible local influence of the obstacle on the scouring dynamics (e.g., see Figures 1b,c). Under these circumstances, both functions v_{sed} and ν lose dependency on the process state, which is the actual rooting depth, L. Moreover, the following assumptions hold: i) the smallest spatial scale of the fluctuations affecting the erosion process is of the order of the sediment grains, and ii) the obstacle size has a negligible effect on the turbulent structure of the flow, so that local entrainment and deposition of sediment particles is equally probable. This allows for assuming the noise term to be uncorrelated and have a symmetric distribution. Hence, we adopt a white gaussian noise modulated by a process variance σ_g^2, $\Xi(t) = \sigma_g^2\xi(t)$. We will validate the assumptions made in Section 3 by using the experimental data from [27,28]. The resulting model with addictive noise reads

$$\frac{dL}{dt} = -v_{sed}(t) + g(t)\xi(t), \qquad t > 0, \tag{2.10}$$

where we put $g(t) = \nu(t)\sigma_g^2$ and $\xi(t)$ is the strength of a Wiener process. This model generates process trajectories alternating deposition and erosion, which mimic the scouring dynamics underlying the type II uprooting (Figure 2). Scouring proceeds until the rooting depth L equals the critical one, L_c. Then, uprooting occurs as a consequence of flow drag balancing the residual mechanical anchoring [27], and the trajectory is lost.

(b) Probability density functions

(i) Rooting depth

As the process is stochastic, we compute the time-dependent probability density function, $p(L,t)$, of observing a given rooting depth L at a time t. Mathematically, this translates into the Master

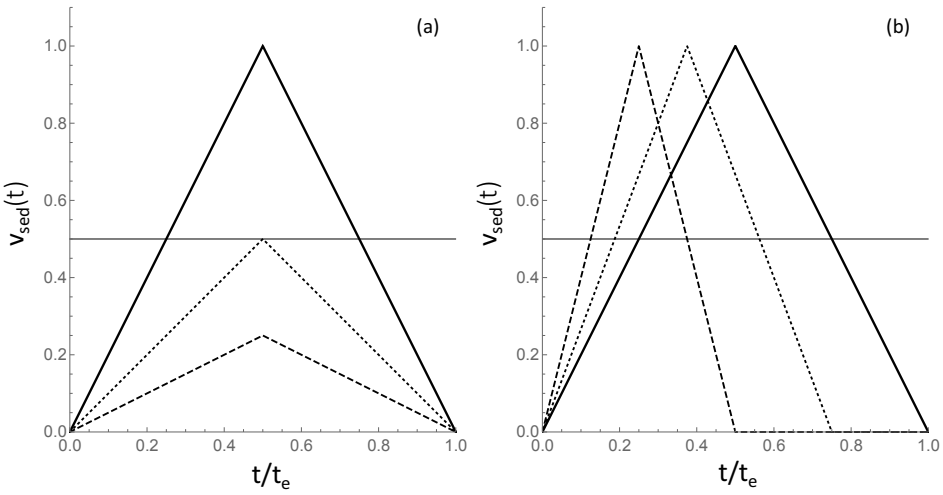

Figure 3. Time dependent functions, $v_{sed}(t)$, used as examples for model solutions for arbitrary length and time scales. The upper panel shows four different v_{sed} functions having same duration and different magnitude. In the lower panel the functions v_{sed} attain the same maximum magnitude and have different duration. for all cases the process variance, i.e. the function g is kept constant and equal to $g = 0.1$ for the whole duration of the process. Other model parameters are $L_0 = 3$, $L_c = 1.5$

equation for a Wiener Process with time-dependent drift, which is better known as Fokker-Planck equation [32]

$$\frac{\partial p}{\partial t} = v_{sed}(t)\frac{\partial p}{\partial L} + \frac{1}{2}g(t)\frac{\partial^2 p}{\partial L^2}, \qquad L \geq L_c. \tag{2.11}$$

This equation has to be supplemented with appropriate initial and boundary conditions. For example, as initial condition at $t = 0$ we impose that the process starts from the rooting depth L_0 for which $p(L_0, 0) = \delta(L - L_0)$. As first boundary condition we impose $p(L, t) = 0$ for $L \to +\infty$, i.e. we allow for particle deposition. This way both sedimentation and erosion may occur although net deposition for which $L > L_0$ becomes less probable as the process evolves. As a second boundary condition, we require that, once a critical rooting depth, L_c, has been reached, then the trajectory is lost, or, physically, the plant is uprooted. Mathematically, $L = L_c$ is an absorbing boundary for which $p(L_c, t) = 0$ [32]; hence, $p(L, t)$ loses mass in time when the process reaches the boundary at $L = L_c$. The solution obtained via the method of images reads [33]

$$p(L,t) = \frac{1}{\sqrt{4\pi G(t)}}\left(e^{\frac{-(L+V(t)-L_0)^2}{4G(t)}} - e^{\frac{V(t)(L_0-L_c)}{G(t)}} - \frac{(L+V(t)-2L_c+L_0)^2}{4G(t)}\right), \tag{2.12}$$

where $G(t) = \int_0^t \frac{g(\tau)}{2} d\tau$, and $V(t) = \int_0^t v_{sed}(\tau) d\tau$, and τ the dummy variable of integration. The mean μ_p and the variance σ_p^2, whose cumbersome expressions are omitted, can easily be obtained analytically from the moment generating function of $p(L, t)$ [32].

We illustrate the process with two examples, where we compare the pdfs of the rooting depth evolution resulting from erosion processes with either constant or time dependent drift functions. We choose time dependent functions with simplified triangular shape for the sake of easier interpretation of the results. The first case is shown in Figure 3a, where the $v_{sed}(t)$ functions have same duration but different peak magnitude, in contrast to those of Figure 3b where $v_{sed}(t)$ has same magnitude but different duration.

At time $t/t_e = 0.25$ (Figure 4a), all pdfs are almost symmetrical and with a mean still around the initial rooting depth, $L/L_0 = 1$, just shifted toward lower L/L_0 values reflecting the erosion intensity of the process. Notice how the pdfs become zero at the boundary $L/L_c = 0.5$ as

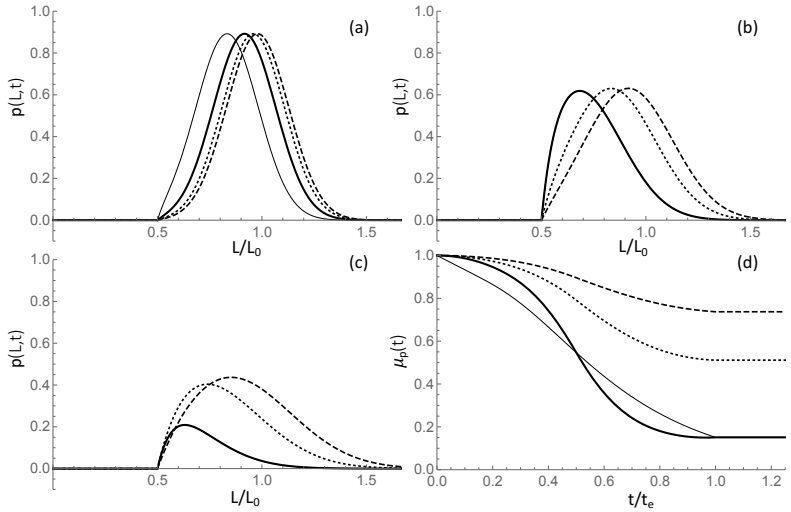

Figure 4. Time dependent evolution of the pdfs, $p(L,t)$ (a-c), and their mean (d) for the erosion processes shown in Figures 3a where $L_0 = 3$ and $L_c = 1.5$. Line thickness and type correspond to the adopted erosion functions. a) t/t_e=0.25; b) t/t_e=0.5; c) t/t_e=1

requested by the absorbing boundary condition. At times $t/t_e = 0.5$ and $t/t_e = 1$ (Figures 4b,c), the effect of the boundary shows up in increasing the skewness of the pdfs and in a loss of probability mass, $\int_{L_c}^{\infty} p(L,t)dL \leq 1$ (see ahead). Notice at these times the pdfs corresponding to the process with constant erosion rate and the one with greatest peak intensity coincide given that the effect of the shape of the erosion function appears within $p(L,t)$ as an integral term, i.e. $V(t)$, only. Clearly, in our simplified model the effect of the drag on the canopy is not included for the time being. The mean of the processes is shown in Figure 4d and clearly illustrates the role of the plants being uprooted in the statistical moment, which stabilises after the erosion process has stopped.

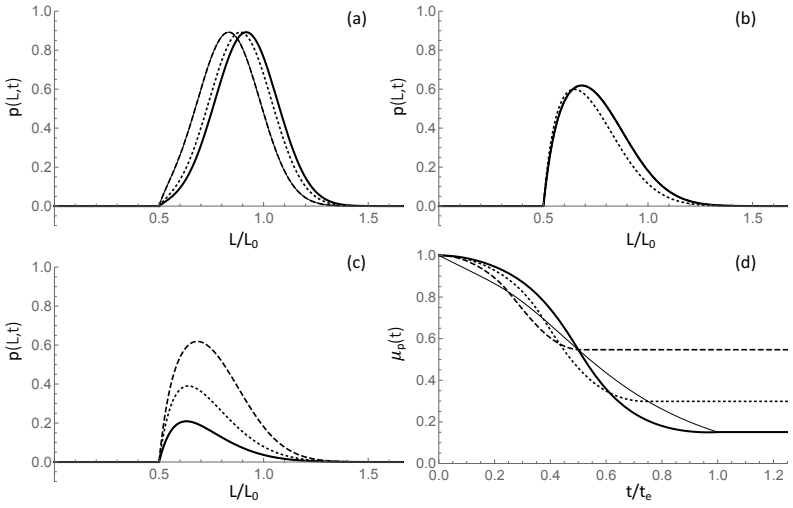

Figure 5. Time dependent evolution of the pdfs, $p(L,t)$ (a,c), and their mean (d) for the erosion processes shown in Figures 3b where $L_0 = 3$ and $L_c = 1.5$. Line thickness and type correspond to the adopted erosion functions. a) t/t_e=0.25; b) t/t_e=0.5; c) t/t_e=1

The distributions and related means resulting from the erosion process of Figure 3b are shown in Figures 5. At time $t/t_e = 0.25$ (Figure 5a) only the continuous erosion process and that having the same integral up to that time show the same pdfs. This results in three coincident pdfs at time $t/t_e = 0.5$ (Figure 5b) when one of the processes has come to stop and the other one is at its maximum erosion rate compared to the process with constant erosion rate. At time $t/t_e = 1$ (Figure 5c) again only three pdfs are visible as two of the processes have the same integral quantities at that time. The time evolution of the mean of the pdf for all processes is shown in Figure 5d.

For practical applications, perhaps more interesting than the solution for $p(L,t)$, is its integral $P(t) = \int_{L_c}^{+\infty} p(L,t)dL$, which is commonly addressed in the literature to as *survivor function* [30]. This function has a true physical meaning in the process as it returns the probability for a plant to have survived the uprooting process up to time t. The evolution of the survivor function in time is shown in Figure 6 and clearly shows how trajectories are lost (i.e., how uprooting occurs) for the type of processes in Figure 3.

(ii) Time-to-uprooting

Closely related to $P(t)$ is the distribution of the uprooting times $p_\tau(T) = -\frac{dP(t)}{dt}$, which corresponds to the pdf of the first mean passage time T across the boundary at $L = L_c$. This pdf depends on L only in the form $L_0 - L_c = L_e$, i.e. the rooting depth responsible for the anchoring exceeding that balanced by the hydrodynamic drag when uprooting occurs. When $P(t)$ cannot be accessed analytically, though numerically, then $p_\tau(T)$ can be obtained by using Laplace transforms as described by [30]. The solution as far as the continuous part of the pdf is concerned reads

$$p_\tau(T) = \frac{L_e e^{\frac{-(L_e - V(T))^2}{4G(T)}} \left(\frac{g(T)}{2} + e^{\frac{(L_e + V(T))^2}{4G(T)}} W(T) \right)}{2\sqrt{\pi} G(T)^{3/2}}, \tag{2.13}$$

where G and V are the previously defined functions calculated at $t = T$ and $W(T) = \sqrt{\pi}\mathrm{Erfc}[\frac{1}{2}G(T)^{-1/2}(L_e + V(T))](v_{sed}(T)G(T)^{1/2} - g(T)V(T)G(T)^{-1/2})$. Notice, that if both functions g and v_{sed} are constant, then $W(T) = 0$ and $p_\tau(T)$ reduces to the well known inverse Gaussian distribution with mean, $\bar{T} = L_e/v_{sed}$, variance, $\sigma_\tau^2 = \frac{L_e g^2}{2v_{sed}^3}$ and power law decay, $t^{-3/2}$ [30,32]. Moreover, if $g(t)$ and $v_{sed}(t)$ are nonzero in the range $0 \le t \le t_e$, then $p_\tau(T)$ is continuous in $0 \le t < t_e$, and has an atom of finite probability equal to $1 - \int_0^T p_\tau(t)dt$ at $T = t_e$.

Solution examples of the resulting $p_\tau(T)$ for the assigned time dependent erosion rate functions of Figures 3 and for two difference magnitude of process noise variance are shown in Figures 7. Notice, that the atom of finite probability (not shown) of $p_\tau(T)$ at the end of the event indicates the percentage of biomass that survived the event and thus corresponds to the integral of $p(L,t_e)$. For increasing noise level the pdf variance and skewness also increase as can be seen from Figures 7a2,b2. Clearly, for a very low noise level compared to the strength of v_{sed} the process is almost deterministic, i.e. the pdf narrows around the mean time to reach the critical erosion amounts, $L_e = L_0 - L_c$.

(iii) Resilience to uprooting

We quantify the statistics of the resilience to uprooting by first computing the scouring energy for a given erosion event, here defined as the energy required for scouring a volume of sediment that exposes the root system at the end of the erosion event, i.e. for $t = t_e$. For a given plant root architecture the volume of soil, V_s containing the roots can be approximated with a function of the rooting depth, i.e. $V_s(L)$ [9]. The scouring energy is here defined as the work done by the stream to transport sediment particles across a path length equal to the root horizontal extension at a certain depth. For the time being we ignore the role of roots on sediment cohesion; the scouring energy thus results into the product of the dimensional critical bed shear stress, τ_c times the

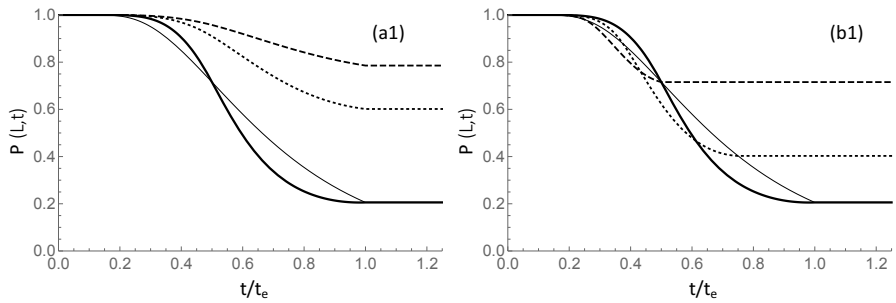

Figure 6. Time evolution of the area of $p(L,t)$ (upper panels) for the erosion processes shown in Figure 3a,b

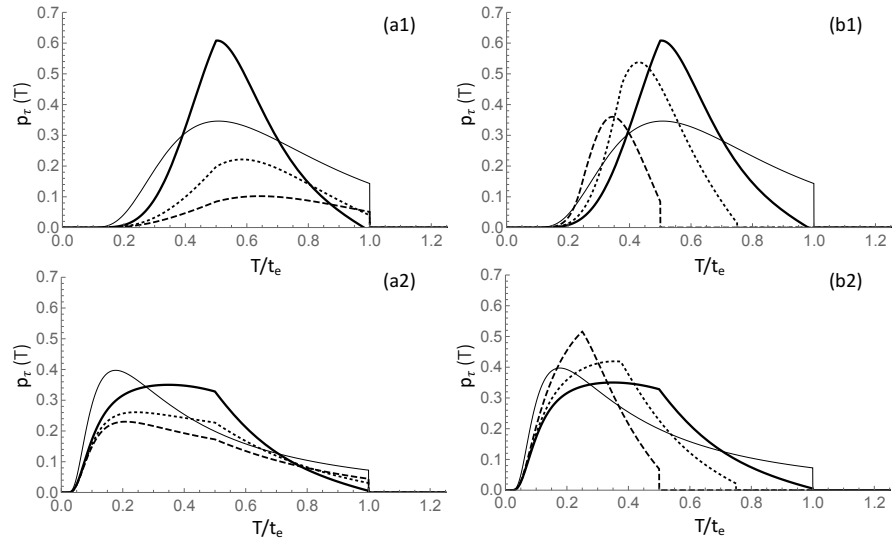

Figure 7. Probability density functions of time-to-uprooting, $p_\tau(T)$ for the erosion processes shown in Figure 3a,b for different magnitude of process variance: a1,b1) g=0.1; a2,b2) g=0.5

scoured volume at a certain time, which we consider here being equal to t_e, that is when the morphodynamic process stops

$$E(L) = \tau_c V_s(L,t), \qquad t = t_e. \tag{2.14}$$

Then, in the domain where the function $E(L)$ is monotonic, we apply the derived distribution approach to map the pdf of residual rooting depth at the end of the process, $p(L)$ into that of the required energy, $p_E(E)$, via the inverted function $L(E)$,

$$p_E(E) = p(L(E)) \| \frac{dL}{dE} \|, \tag{2.15}$$

where the derivative term is the Jacobian of the transformation that renormalizes the distribution. The resilience to uprooting can be defined as the integral of this distribution at the end of the process, i.e. for $t = t_e$

$$R = \int_{E(L_0)}^{E(L_c)} p_E(E) dE, \tag{2.16}$$

whose general solution reads

$$R(0 \le E \le E(L_c)) = \frac{1}{2}\left(Erf[A] - Erf[A(1-B)] + e^{2AC}\left(-Erf[A+C] + Erf[(A+C)(1-D)]\right)\right), \tag{2.17}$$

where

$$A = \frac{V(T)}{2\sqrt{G(T)}}; \quad B = \frac{6^{2/3}\left(\frac{E(L_c)}{\tau_c}\right)^{1/3}}{V(T)\pi^{1/3}}; \quad C = \frac{L_0 - L_c}{\sqrt{G(T)}}; \quad D = \frac{6^{2/3}\left(\frac{E(L_c)}{\tau_c}\right)^{1/3}}{(V(T)+2(L_0-L_c))\pi^{1/3}}. \tag{2.18}$$

The function R represents the probability that the energy required for reducing the rooting depth, L to the critical depth, L_c is larger than the energy spent by the stream during the whole erosion event. As resilience depends on the effective rooting depth, $L_e = L_0 - L_c$, and on the shape of the volume of soil englobing the roots, it varies between 0 (purely deterministic uprooting) to 1 (purely deterministic survival) depending on whether L_e is small or big compared to the potential average scouring $V(t_e) = \int_0^{t_e} v_{sed}(\tau)d\tau$, respectively. Hence, by following [16] and using information theory we also define the predictability of plant uprooting by flow as the Shannon entropy of the binary variable [34] R, representing the resilience to uprooting or survival

$$H = -R\log_2 R - (1-R)\log_2(1-R). \tag{2.19}$$

The function H is plotted in Figure 8 for the reference process events of Figures 3 (upper panels) and by assuming that root architecture is contained in a conical soil volume with aperture angle of 60° as shown in Figure 8 (left panel).

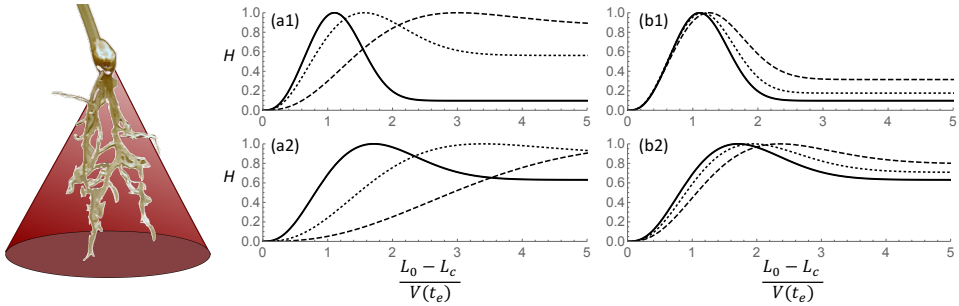

Figure 8. Exemplary root scheme used to compute the prediction entropy, H as a function of dimensionless effective rooting depth vs scouring depth ratio, $(L_0 - L_c)/V(t_e)$. The four panels show the prediction entropy for the erosion processes shown in Figure 3a,b and different magnitude of process variance: a1,b1) g=0.1; a2,b2) g=0.5

The function H is plotted as a function of the ratio between the effective rooting depth, $L_e = L_0 - L_c$ and the potential scouring, $V(t_e)$ of the given morphodynamic event. When such a ratio is small, then the rooting depth is small compared to potential scouring and so is the resilience to uprooting; uprooting is then practically deterministic, hence the low prediction entropy. A big ratio indicates high resilience to uprooting and the prediction of survival is again deterministic although conditioned by the process variance, whose increase makes the prediction entropy to also increasing. In between such extremes, that is when the rooting depth is of the same magnitude of the potential scouring, than the prediction is the worst. This can be better understood when considering an hypothetical purely deterministic erosion process with zero process noise. In this case the prediction entropy would degenerate into a peak of unitary magnitude at $(L_0 - L_c)/V(t_e) = 1$, which separates the region of purely deterministic (i.e., certain) uprooting from that of purely deterministic (i.e., certain) survival to the left and to the right of the peak, respectively.

Table 1. Flow velocity, v, discharge, Q, water depth, Y, equilibrium slope, i_{eq} and vertical erosion velocity, v_{sed} for the four flow settings tested.

	Setting 1	Setting 2	Setting 3	Setting 4
Q (l s^{-1})	1.60	1.81	1.94	2.15
i_{eq} (%)	2.4	2.7	3.0	3.5
v_{sed} (mm s^{-1})	0.043	0.058	0.076	0.100
v (computed) (m s^{-1})	0.49	0.53	0.57	0.61
v (measured) (m s^{-1})	0.49	0.56	0.54	0.57
Y (mm)	11.0	11.4	11.9	11.7

3. Model validation

Measuring plant uprooting by flow both at field and laboratory scales requires monitoring of the riverbed evolution while erosion proceeds, and the recovery of the uprooted plants. To our knowledge no complete dataset exists in the literature other than that concerning *Avena sativa*, as recently presented by [27]. *Avena sativa* has been much studied as a model for riparian vegetation [22,35] thanks to its simple root structure and small stem size, i.e. comparable to the typical sediment grain size used in laboratory experiments. Anchoring forces have also been investigated [18,21,28], and in the recent pioneering experiment by [27] the evolution of the bed elevation has been monitored and the uprooted plants collected. This makes the dataset unique for validating our model, whose implications can be expected to be significant for field situations.

From the experimental data of [27,28] the measured time-to-uprooting, T is plotted against the length of the main root for all tested seedlings (Figure 9). Besides noticing the variability in the data itself, it can be seen that T increases in average with decreasing flow magnitude and increasing root length, as expected.

In their experiments, Edmaier et al. [27] studied the Type II mechanism of uprooting by flow for small values of the obstacle to sediment size ratio, i.e. for which the obstacle induced scouring is negligible compared to the non-local scour. Under such conditions, the riverbed erosion rate can be assumed independent of the presence of the obstacle, and the noise affecting the process to be mainly additive in nature. This essentially reflects the hydrodynamic effects on both the erosion and the drag, as well as the heterogeneity of plant root architecture and biomechanical characteristics.

The issue that makes type II uprooting difficult to capture is that L_0 and L_c vary for each plant, and upon the variation of v_{sed}. The variation of L_c occurs indirectly upon variation of L_0 and v_{sed}. That is, because of the correlation between above and below ground biomasses [28,29], different root length L_0 yield different values of flow drag as different v_{sed} correspond to different flow velocities. In the dataset by Edmaier et al. [27], this is reflected by the presence of a linear correlation between L_c and L_0 (Pearson correlation coefficient of 0.8). However, when considering $\tilde{L}_c = L_c/L_0$, the correlation with v_{sed} almost vanishes (Pearson correlation coefficient of 0.027). This suggests rewriting equation (2.11) in the dimensionless form

$$\frac{\partial p}{\partial \tilde{t}} = \frac{\partial p}{\partial \tilde{L}} + \frac{\sigma^2}{2L_0 v_{sed}} \frac{\partial^2 p}{\partial \tilde{L}^2}, \tag{3.1}$$

where we have introduced the dimensionless variables $\tilde{t} = \frac{t v_{sed}}{L_0}$ and $\tilde{L} = \frac{L}{L_0}$ given that $L_e \sim L_0$ for the data being considered. This way, it is possible to aggregate the empirical statistics obtained for different rooting depth L_0. The residual correlation between $\tilde{L}_c$ and v_{sed} (Pearson correlation coefficient of 0.22) introduced by how flow drag changes with vegetation development can be accounted for by using a different $\tilde{L}_c$ for each of the four flow settings (corresponding to four different v_{sed}).

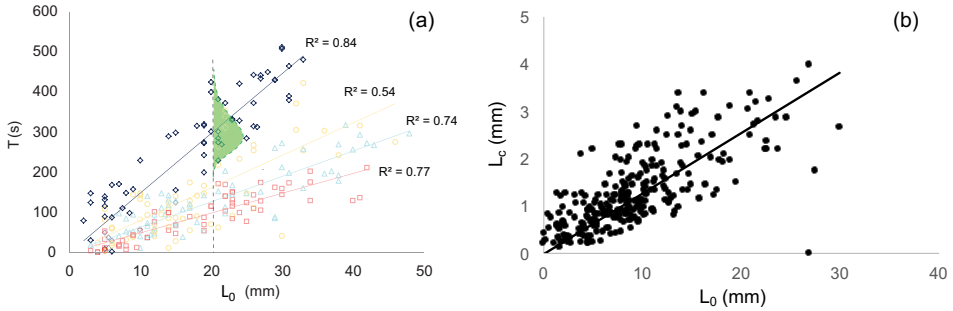

Figure 9. (a) Time-to-uprooting T plotted against length of the main root L_0 for the four investigated flow settings (flow discharge Q_1 (dark blue diamonds) $< Q_2$ (orange circles) $< Q_3$ (turquoise triangles) and $< Q_4$ (red squares)). (b) Empirical linear correlation between L_c and L_0, which can be removed by normalizing the data to L_0.

For constant v_{sed} and σ^2, Eq.(2.13) reduces to the inverse Gaussian distribution, also known as Wald distribution [32,36]. As a result, the distribution $p_\tau(\tilde{T})$ of the dimensionless time-to-uprooting $\tilde{T} = \frac{T v_{sed}}{L_0}$ is given by

$$p_\tau(\tilde{T}) = \frac{e^{-\frac{(1-\tilde{T})^2}{2\tilde{\sigma}^2\tilde{T}}}}{\sqrt{2\pi\tilde{T}^3}\tilde{\sigma}}, \tag{3.2}$$

where $\tilde{\sigma}^2 = \frac{\sigma^2}{L_0 v_{sed}}$. Notice, that this dimensionless variance plays the role of a Peclét number for the advection-diffusion of uprooting probability. Hence, when $\tilde{\sigma} << 1$, then the action of the deterministic drift prevails on the process noise, and viceversa.

The comparison between the theoretical cumulative distribution

$$P_\tau(\tilde{T}' \leq \tilde{T}) = \int_0^{\tilde{T}} p_\tau(\tilde{T}')d\tilde{T}' \tag{3.3}$$

of the dimensionless time-to-uprooting and the corresponding empirical distribution is presented in Figure 10a.

One readily notices the mismatch for short times, where uprooting of type I for which noise dominates and uprooting occurs without scouring [25] rather than of type II occurs. Calibrating the mode of the distribution instead of the average (given by v_{sed}) would result in a better match between theoretical and empirical statistics for the longer times, where type II uprooting is the relevant uprooting mechanism. However, although the hypothesis of uncorrelated Gaussian noise to describe the random fluctuations affecting the dynamics is rather crude, the proposed stochastic model already captures the main features of the empirical statistics. Moreover, for the experimental data being analyzed our model confirms a coefficient of variation ($\tilde{\sigma}_\tau/\tilde{\bar{T}}$) equal to 0.48, which indicates the ratio between the stochastic and the deterministic components affecting the uprooting process. As $\tilde{\bar{T}} \sim 1$, then the coefficient of variation is equal to the standard deviation of the process.

The corresponding prediction entropy, H, calculated for all the data at the time when uprooting occurs and the process stopped (i.e., for $t = T$), scales according to the ratio $V(T)/\sqrt{(G(T))}$ (Figure 10b). At this time $V(T) = L_e = L_0 - L_c$ and the coefficients, A, B, C, D of Equation (2.17) depend solely on the integral quantities $V(T)$ and $G(T)$ that represent the total scouring and the integrated variance to uprooting, respectively. Hence, the uprooting dynamics is more predictable for less resilient plants exposed to erosion processed that result in low $V(T)/\sqrt{(G(T))}$ and viceversa. Data are shown in colours for three ranges of the ratio $V(T)/\sqrt{(G(T))}$, whose correspondence in real coordinates L_0 and T is shown in the inset panel. It is important to notice that the data points in Figure 10b would appear as a point at $(L_0 - L_c)/V(T) = 1$ in the prediction entropy plot of Figure 8 for the corresponding H. Thus, for

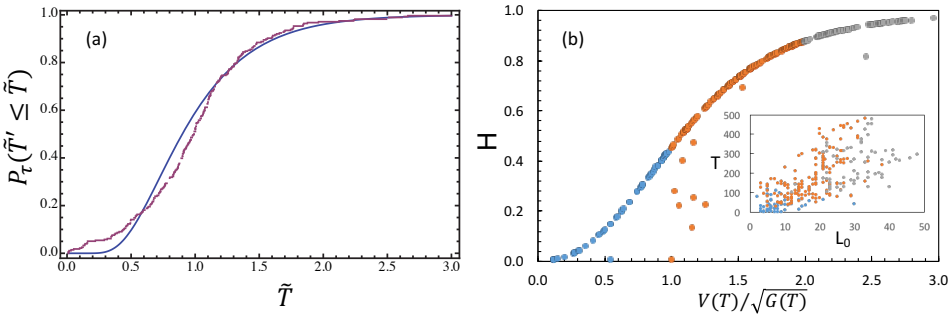

Figure 10. a) Comparison between the theoretical (blue) and the empirical (magenta) cumulative density functions of the dimensionless time-to-uprooting $\tilde{T} = \frac{T v_{sed}}{L_0}$; b) Prediction entropy for the empirical dataset computed at the instant, T when uprooting occurred. The blue, orange and grey colours represent the variable $V(t)/\sqrt{G(t)}$ in the ranges 0÷1, 1÷2 and 2÷3, respectively. The inset panel shows how the same empirical data would appear in the time-to-uprooting, T, vs the root length, L_0 plot.

same erosion rate, v_{sed}, as the integral variance of the process increases, the prediction entropy would decrease for plant with short roots and viceversa.

4. Discussion and conclusions

We derived a theoretical model describing vegetation uprooting by flow and related statistics under generic time-dependent flow erosion conditions. The survivor function, which is obtainable by integration of Eq. (2.12), provides the fraction of plants that survives uprooting during a given erosion event (e.g., Figure 1). From a biological point of view, this function indicates the fraction of plants the have the chance to recover partial erosion before the occurrence of the next flooding event. This competition between growth and uprooting where vegetation compensates with root growth the reduction of anchorage between successive flooding events has been observed in the field, and is described by [29]. In its simplicity, the adopted physical approach helps to explain situations such as those shown in Figure 1, and provides mathematical relationships for quantitative calculations of both river engineering and ecological relevance. For example, our analytical model could be introduced in numerical morphodynamic models [37] together with some recent analytical models for the root density distribution [8] in order to obtain the first probabilistic description of plant uprooting by flow in riparian corridor ecomorphodynamics.

The resilience to uprooting and the prediction entropy can also be calculated starting from the rooting depth and the expected scouring dynamics. Generally, plant resilience to uprooting by flow following on sediment erosion depends on the effective rooting depth vs potential scouring ratio and increases according to this ratio. The corresponding ability to predict uprooting depends on the variance of the erosion process and is described by the prediction entropy function. Hence, for an erosion process with low variance plants with rooting depth vs potential scouring ratio greater than 1 are highly resilient and uprooting is unlikely to occur with a high prediction confidence (i.e., low prediction entropy). Increasing the erosion process variance would reduce the resilience, increase the prediction entropy and consequently reduce the reliability of the prediction about uprooting occurrence.

In the correspondence between the uprooting dynamics involving the soil-root system [27] and the fatigue mechanism leading to the failure of materials [38,39], our model suggests that root anchoring plays the role of the strength of material. Based on the form of Eq. (2.9), the overall dynamics of the Type II uprooting mechanism allows for linking the cdf of the energy required for uprooting to plant resilience to uprooting. As uprooting occurs as an integrated stochastic process and not simply as an over-threshold event, the resilience to uprooting can thus be ascribed to the

memory of the plant-soil system that is stored by roots. This picture classifies extreme events as the ones leading to actual uprooting as a result of the combined random and deterministic dynamics of the stochastic scouring process.

In conclusion, this model proves in a simple way that the rooting depth does not solely explain the statistics and the time-to-uprooting for riverbed vegetation. This explains the results of the experiments of Edmaier *et al.* [27], which inspired this work. Given the stochastic nature of riverbed erosion process, the critical scouring depth is reached at different times even at constant erosion rates. Thus, computing the return time for plant uprooting based on the return time of hydrological events might not entirely be correct depending on the relative importance of the deterministic and the random components of the erosion process. The model provides the distribution of uprooting times and this should be the starting point to redefine the theory of extreme events for ecosystem processes, which typically show a memory type of evolution dynamics.

Data Accessibility. The dataset from Edmaier et al. is fully available as spreadsheet (please, see supplementary material).

Authors' Contributions. PP developed the model and wrote the paper; BC analyzed the experimental data and helped preparing the Figures.

Competing Interests. We declare we have no competing interests.

Funding. This work had no funding support.

Acknowledgements. We thank Katharina Edmaier for providing the data, Amilcare Porporato for fruitful discussion about memory effects in stochastic processes, and Alistair Borthwick for proofreading the manuscript.

Disclaimer. This work did not involve any active collection of human data, but only flume erosion experiment data from Edmaier et al [27].

References

1. Higler L. 2009. Biology and biodiversity of river systems, in *Encyclopedia of Life Support Systems - Fresh surface water*, edited by J. C. I. Dooge, vol. II, pp. 222–23, UNESCO, 2009.
2. Mahoney JM, Rood SB. 1998. Streamflow requirements for cottonwood seedling recruitment – an integrative model, *Wetlands*, **18**, 634–645.
3. Samuelson GM, Rood SB. 2004. Differing influences of natural and artificial disturbances on riparian cottonwoods from prairie to mountain ecoregions in Alberta, Canada, *Journal of Biogeography*, **31**, 435–450.
4. Camporeale C, Perucca E, Ridolfi L, Gurnell A. 2013. Modeling the interaction between river morphodynamics and riparian vegetation, *Reviews of Geophysics*, **51**, 1–36.
5. Gurnell A. 2013. Plants as river system engineers, *Earth Surf. Proc. Land.*, **39**, 4–25.
6. Gibling M, Davies N. 2012. Palaeozoic landscapes shaped by plant evolution, *Nature Geocience*, **5**, 99–105, 2012.
7. Pasquale N, Perona P, Francis AR, Burlando P. 2012. Effects of streamflow variability on the vertical root density distribution of willow cutting experiments, *Ecol. Eng.*, **40**, 167–172.
8. Tron S, Perona P, Gorla L, Schwarz M, Laio F, Ridolfi L. 2015. The signature of randomness in riparian plant root distributions, *Geophys. Res. Lett.*, **42**, 7098–7106.
9. Gregory P. 2006 *Plant roots, Growth, activity and interaction with soils*, Blackwell Publishing Ltd.
10. Pasquale N. 2012 *Quantification of vegetation root induced cohesion in non-cohesive river beds by experiments, monitoring and modeling*, Ph.D. thesis, ETH Zürich, Switzerland.
11. Polvi L, Wohl E, Merritt DM. 2014. Modelling the functional influence of vegetation type on streambank cohesion, *Earth Surf. Process. Landforms*, **39**, 1245–1258.
12. Edmaier K, Burlando P, Perona P. 2011. Mechanisms of vegetation uprooting by flow in alluvial non-cohesive sediment, *Hydrology and Earth System Sciences*, **15**, 1615–1627.
13. Kui L, Stella J, Lightbody A, Wilcox AC. 2014. Ecogeomorphic feedbacks and flood loss of riparian tree seedlings in meandering channel experiments, *Water Resour. Res.*, **50**, 9366-9384.
14. Bywater-Reyes S, Wilcox AC, Stella JC, Lightbody AF. 2015. Flow and scour constraints on uprooting of pioneer woody seedlings, *Water Resour. Res.*, **51**, 9190–9206.

15. Ridolfi L, D'Odorico P, Laio, F. 2011. *Noise-induced phenomena in the environmental sciences.* Cambridge, UK: Cambridge University Press.
16. Perona P., Daly E., Crouzy B., Porporato A. 2012. Stochastic dynamics of snow avalanche occurrence by superposition of Poisson processes. *Proc. R. Soc. A*, **468**, 4193-4208
17. Ennos R. 2000. The mechanics of root anchorage, *Advances in Botanical Research*, **33**, 133-157.
18. Edmaier K, Crouzy B, Ennos R, Burlando P, Perona P. 2014. Influence of root characteristics and soil variables on the uprooting mechanics of *Avena sativa* and *Medicago sativa* seedlings, *Earth Surf. Proc. Land.*, **39**, 1354–1364.
19. Schwarz M, Cohen D, Or D. 2010. Root-soil mechanical interactions during pullout and failure of root bundls, *Journal of Geophysical Research*, **115**, F04,035.
20. Schwarz M, Cohen D, Or D. 2011. Pullout tests of root anchorage and natural bundles in soil: Experiments and modelling, *Journal of Geophysical Research*, **116**, F02,007.
21. Crouzy B, Edmaier K, Perona P. 2014. Biomechanics of plant anchorage at early development stage, *Journal of Theoretical Biology*, **363**,22–29.
22. Perona P, Molnar P, Crouzy P, et al. 2012, Biomass selection by floods and related timescales: Part 1. Experimental observations, *Adv. Water Res.*, **39**, 85-96.
23. Crouzy B, Edmaier K, Pasquale N, Perona P. 2013. Impact of floods on the statistical distribution of riverbed vegetation, *Geomorphology*, **202**, 51–58.
24. Nepf H. 2012. Flow and transport in regions with aquatic vegetation, *Annu. Rev. Fluid Mech.*, **44**, 123–142.
25. Crouzy B, Perona P. 2012. Biomass selection by floods and related timescales. Part 2: Stochastic modelling, *Adv. Water Res.*,**39**, 97–105.
26. Vesipa R, Camporeale C, Ridolfi L. 2016. Recovery times of riparian vegetation, *Water Resour. Res.*, *52*, 1-17.
27. Edmaier K, Crouzy B, Perona P. 2015. Experimental characterization of vegetation uprooting by flow, *J. Geophys. Res. Biogeosci.*, **120**, 1–13.
28. Edmaier K. 2014 *Uprooting mechansims of juvenile vegetation by flow erosion*, Ph.D. thesis, Swiss Federal Institute of Technology, Lausanne, CH.
29. Pasquale N, Perona P, Francis RA, Burlando P. 2014. Above-ground and below-ground salix dynamics in response to river processes, *Hydrological Processes*, **28**, 5189–5203.
30. Daly E, Porporato A, State-dependent fire models and related renewal processes, *Phys. Rev. E*, **74**, 041,112–117.
31. Melville BW, Sutherland A. 1988. Design method for local scour at bridge piers., *Journal Hydr Eng ASCE*, **114**, 1210–1226.
32. Cox D, Miller H. 1965 *The Theory of Stochastic Processes*, Methuen, London, 1965.
33. Polyanin AD. 2002 *Linear partial differential equations for engineers and scientists*, Chapman & Hall/CRC, NewYork.
34. Cover, TM, Thomas, JA. 2006 *Elements of information theory*, 2nd edn. New York, NY: Wiley Interscience
35. Clarke L. 2014. The use of live vegetation in geomorphological experiments: how to create optimal growing conditions, *Earth Surface Processes and Landforms*, **39**, 705–710.
36. Katul G, Porporato A, Nathan R, Siqueira M, Soons M, Poggi D, Horn H, Levin S. 2005. Mechanistic analytical models for long-distance seed dispersal by wind, *American Naturalist*, **166**, 368–381.
37. Bertoldi W, Siviglia A, Tettamanti S, Toffolon M, Vetsch D, Francalanci S. 2014. Modelling vegetation controls on fluvial morphological trajectories, *Geophys. Res. Lett.*, **41**.
38. Leverett L, Lynch E, Alfrey J, Hellums CP. 1972. Red blood-cell damage by shear-stress, *Biophysical Journal*, **12**, 257–273, 1972.
39. Tillmann W, Reul H, Herold M, Bruss KH, van Gilse J. 1984. In-vitro wall shear measurements at aortic valve prostheses, *Journal of Biomechanics*, **17**, 263–279.